AST5220 Cosmology II

Milestone 4 - Computing the CMB Power Spectrum

Jakob Borg

June 9, 2020

1 Introduction

This is the final milestone of our four part project to compute the cosmic microwave background (CMB) power spectrum, expressed through C_ℓ. Here we build upon the results from the three previous milestone where we computed the background evolution and expansion of the Universe [Borg, 2020a], the ionization history, the optical depth and visibility function [Borg, 2020b] and last the evolution of the perturbations set up by inflation [Borg, 2020c].

The full project can be found on GitHub, here are link to the projects main directory[1]. All computation and calculations are done in "C++", with the source code found here[2]. The main calculations for this milestone may be found in *PowerSpectrum.h*, building upon everything we have done so far. As mentioned in Borg [2020c] we will need one specific quantity, the source function, which we will implement in the code from the last milestone in *Perturbations.h*.

2 Theoretical Background

2.1 The CMB Power Spectrum

The CMB power spectrum is the main goal of our calculations, described through C_ℓ. This gives us a statistical representation of how much the different perturbations of varying scales contributes to the temperature map we observe when measuring the CMB. The angular scales ℓ are today related to the physical scale in Fourier space characterized through the wavenumber of the perturbations k, following

$$\ell \sim k\eta_0$$

where η_0 is the conformal time today.

The measured temperature can be expanded into spherical harmonics as

$$T(\hat{n}) = \sum a_{\ell m} Y_{\ell m}(\hat{n}) \tag{1}$$

where $Y_{\ell m}(\hat{n})$ are the spherical harmonics and $a_{\ell m}$ are the coefficients. The power spectrum it self is defined as the expectation value of the squared coefficients, which is the same as the variance as the coefficients are gaussian with zero expectation value,

$$C_\ell = \left\langle |a_{\ell m}|^2 \right\rangle = \langle a_{\ell m} a^*_{\ell m} \rangle \,.$$

[1] URL: `https://github.com/Lilleborg/AST5220-Cosmology2/tree/master/Numerical_projects`
[2] URL: `https://github.com/Lilleborg/AST5220-Cosmology2/tree/master/Numerical_projects/src`

But instead of finding the $a_{\ell m}$s we can use what we have from Borg [2020c], where we expressed the temperature of the CMB $T(\hat{n})$ in terms of the photon multipoles Θ_ℓ. Expressing the square of $a_{\ell m}$s through the square of the multipoles, using the primordial power spectrum to scale the multipoles and integrating over all the spatial directions we find the full expression for the power spectrum today

$$C_\ell(k, x=0) = 4\pi \int_0^\infty A_s \left(\frac{k}{k_{\text{pivot}}}\right)^{n_s-1} \frac{\Theta_\ell^2(k, x=0)}{k}\, \mathrm{d}k \tag{2}$$

where we have assumed an isotropic Universe, the scaling is done to adjust the simplified initial conditions for the differential equation system for the multipoles as discussed in Borg [2020c] and

$$\frac{k^3}{2\pi^2} P_{\text{primordial}}(k) = A_s \left(\frac{k}{k_{\text{pivot}}}\right)^{n_s-1}. \tag{3}$$

Here A_s is the amplitude, n_s is the spectral index and k_{pivot} is some scale for which the amplitude of the spectrum is A_s. As we want to reproduce the power spectrum as we see it today, we use the todays value of the multipoles at $x = 0$.

2.1.1 The Line of Sight Integration

In order to solve eq. (2) from large scales, low ℓ, to small scales, high ℓ, we need all the multipoles for the corresponding scales we whish to compute. As discussed in Borg [2020c] this is not solved through the endless hierarchy of Boltzmann equations for the multipoles. Instead we utilize the line of sight integration approach of Zaldarriaga and Seljak, which formally integrates the equation for $\dot{\Theta}$ and does the multipole expansion at the end. After some details this gives us a final expression for the different multipoles, which can be solved directly without the hierarchy

$$\Theta_\ell(k, x=0) = \int_{-\infty}^0 \tilde{S}(k, x) j_\ell\left(k\eta_0 - k\eta\right) \mathrm{d}x\,. \tag{4}$$

Here j_ℓ is the spherical Bessel function evaluated at $k\eta_0 - k\eta(x)$, which projects the 3D field of the perturbations onto the 2D sphere we observe. $\tilde{S}$ is the aforementioned source function, which describes the physical effects changing the photons energies as it travels through the Universe to us. The source function is defined as

$$\tilde{S}(k, x) = \tilde{g}\left[\Theta_0 + \Psi + \frac{1}{4}\Pi\right] + e^{-\tau}\left[\Psi' - \Phi'\right] - \frac{1}{ck}\frac{d}{dx}(\mathcal{H}\tilde{g}v_b) + \frac{3}{4c^2k^2}\frac{d}{dx}\left[\mathcal{H}\frac{d}{dx}(\mathcal{H}\tilde{g}\Pi)\right] \tag{5}$$

following Callin [2006]. All the involved quantities for the source function is calculated and discussed in the previous milestones. As discussed in Borg [2020c] we don't include polarization in our computations, so $\Pi \equiv \Theta_2$. The last term can be rewritten using the chain rule to

$$\begin{aligned}\frac{d}{dx}\left[\mathcal{H}\frac{d}{dx}(\mathcal{H}\tilde{g}\Pi)\right] = \Pi\tilde{g}\left(\mathcal{H}\ddot{\mathcal{H}} - \dot{\mathcal{H}}^2\right) \\ + 3\mathcal{H}\dot{\mathcal{H}}\left(\dot{\tilde{g}}\Pi + \tilde{g}\dot{\Pi}\right) \\ + \mathcal{H}^2\left(\ddot{\tilde{g}}\Pi + 2\dot{\tilde{g}}\dot{\Pi} + \tilde{g}\ddot{\Pi}\right).\end{aligned}$$

The physical effects described by the source function can be seen from the four different terms

1 The Sachs Wolfe effect, the main contribution to the power spectrum, is the effective monopole $\Theta_0^{\text{eff}} = \Theta_0 + \Psi + \frac{1}{4}\Pi$, describing the average temperature of the photons with the effect of climbing out of the gravitational potential Ψ and with a small correction due to polarization in Π. This term is weighted by the visibility function, which essentially works as a Dirac Delta function at the time of recombination, effectively picking out the value of the effective monopole at the last scattering surface (LSS). This makes sense as we know the photons decouple after recombination and free steam to us, so we are actually observing the effective monopole at LSS.

2 The integrated Sachs wolf effect, the effect on photons traveling through gravitational potentials that are changing in time. As we saw in Borg [2020c] this is non-negligible during the period where small scale perturbations enter the horizon right before recombination, and in later times when large scale perturbations enter the horizon in the dark energy dominated era. As the term is weighted with the exponential of the optical depth, $e^{-\tau}$, this term is not contributing much before recombination, where $\tau > 1$, and thus the late integrated Sachs Wolf effect, from the largest scales, is the main contributor from this term.

3 The third term is a doppler term, which describes the doppler effect on the photons from the slightly different peculiar velocities the perturbations have in the tight coupling regime, where photons and baryons are coupled and in thermal equilibrium due to the high optical depth. This term is again weighted by the visibility function and its derivatives, effectively giving us a contribution from this term at the LSS.

4 The last term is small, and describes a small quadrupolar correction to the source function, again weighted by the visibility function and its derivatives.

2.2 Matter Power Spectrum

Last we have the matter power spectrum defined as

$$P_i(k,x) = |\Delta_i(k,x)|^2 P_{\text{primordial}}(k) \tag{6}$$

where $P_{\text{primordial}}(k)$ is the primordial power spectrum from eq. (3) and Δ_i is the gauge invariant density perturbation defined as

$$\Delta_i = \delta_i - \frac{3(1+\omega_i)\mathcal{H}}{ck} v_i \tag{7}$$

where ω_i is the equation of state for component i. Our main goal is the full matter power spectrum, for components $i =$ baryons and CDM . For the total matter we have the invariant density

$$\Delta_M \equiv \frac{c^2 k^2 \Phi(k,x)}{\frac{3}{2}\Omega_{M,0} a^{-1} H_0^2}. \tag{8}$$

For these results we also want to point out the equality scale, k_{eq}. This marks the scale corresponding to the peak in the power spectrum due to the smaller scales entering the horizon in the radiation dominated regime being suppressed by the Meszaros suppression. The equality scale is found by

$$k_{\text{eq}} = \frac{a_{\text{eq}} H(a_{\text{eq}})}{c}, \tag{9}$$

where a_{eq} is defined as the time where $\Omega_R = \Omega_M$, and can be approximated as $a_{\text{eq}} \approx \frac{\Omega_{R,0}}{\Omega_{M,0}}$. The last approximation can be found by assuming only radiation and matter as energy contributors in the Universe, which is reasonable in the early Universe where the equality happens.

3 Method

3.1 Data Grids and Resolution

As with the other milestones we have to define a grid for our computations. But in this milestone we have a few different grids to keep track of; the logarithmic scale factor, x, to solve eq. (4), for wavenumber, k, to solve eq. (2), and finally the angular scale, ℓ, to solve the power spectrum for the different scales we want to compute. Taking computation time and precision into account, we have through experimentation found some reasonable data grids to do our computation over. As for the other milestones, our end goal is to compute the quantities we need in the defined grids, and then spline the result to get an even finer resolution in our final result. The experimentation was done by gradually increasing the number of points in our grids until the result was comparable to our testing data, more on that in appendix A. We then increased the number of point further until we had more results to compare, before gradually reducing the number of points for each quantity as long as there was negligible loss in precision.

To optimize our computation time, we use a uneven resolution in our logarithmic scale factor grid. As discussed in section 2.1.1 we are most interested in the time around the LSS. Inspired by Callin [2006], we create a linearly spaced range from $x_{\text{start}} = -15$ to the point where the visibility function start to increase around recombination at x_{rec}, defined as where the free electron fraction reaches $X_e(x_{\text{rec}}) = 0.5$. In this range we use 15 data points. Then during recombination and until the visibility function reaches $\tilde{g}(x) < 0.1$ we use 170 data points. Finally, from after this point and until today at $x = 0$ we again use 15 points, resulting in only 200 x-grid points total, which greatly increases the computation time.

To keep a high order of precision we found that we had to use a large number of k-grid points to solve eq. (2). In the end we used 2000 grid points, logarithmically spaced from $k_{\min} = 5 \times 10^{-5}\,\mathrm{Mpc}^{-1}$ to $k_{\max} = 0.3\,\mathrm{Mpc}^{-1}$.

Finally our angular scale grid, we use the provided[3] range of values. As discussed in section 2.1.1, we don't need to solve the spectrum for linearly spaced ℓ all the way from large scales to small scales. We therefore use linearly spaced values for all the largest scales, 2 to 8, before gradually increasing the spacing between the values from 2, to 3, 5, 10, 20, 25 and eventually 50 for the smallest scales up to $\ell_{\max} = 2000$.

3.2 Precalculating The Spherical Bessel Function

In order to solve eq. (4) to a high order of precision we need to evaluate the highly oscillating spherical Bessel function in the same integral. As this function is so sensitive and oscillating, we need to to solve it in a higher resolution grid than what is described in section 3.1 for the logarithmic scale factor. As discussed we save a lot of computation time by having our sparsely populated time array, as we mostly need high resolution during recombination, but thats not the case for the spherical Bessel function. It peaks around $j_\ell(z \approx \ell)$, being highly oscillatory with dampening after this point. We therefore precalculate all the Bessel functions we need for the desired ℓ-values with a much higher resolution in the argument to the Bessel function, $z \in [0, 5000]$ with 10000 grid points, and then spline the results. These splines are then used to solve eq. (4) in the reduced resolution, now with the splines being evaluated at $j_\ell(k\eta_0 - k\eta(x))$ to a high precision. This ends up saving us a lot of computation time, as we don't have to evaluate the entire source function at the same resolution as we need for the precalculation of the Bessel function, and creating all the splines we need only takes about $\sim 4.6\,\mathrm{s}$.

3.3 Solving the CMB Power Spectrum

With the Bessel functions splined, we are ready to take on eqs. (2) and (4). For both equations we rewrite the integral into a differential equation, and use the ODE-Solver we have used in all the previous milestones to solve the equations. For these equations we have used a higher precision for the solver with an initial timestep of 1×10^{-3}, absolute error of 1×10^{-10} and relative error of 1×10^{-10}, with the explicit embedded Runge-Kutta-Fehlberg (4,5) method from the GSL-library [gsl, 2020].

3.3.1 Line of Sight Integration

To solve eq. (4) as a differential equation we rewrite the equation into the following form

$$\frac{\mathrm{d}\Theta_\ell(k,x)}{\mathrm{d}x} = \tilde{S}(k,x) j_\ell\left[k\eta_0 - k\eta(x)\right] \tag{10}$$

with initial conditions for all scales k being zero, as the multipoles are assumed to be zero at $x \to -\infty$,

$$\Theta_\ell(k, x \to -\infty) = 0.$$

This is solved in the mentioned x-grid, for all the values of ℓ and k. The result is extracted today at $x = 0$, and splined as a 2D spline over angular scale and wavenumber.

In order to get a better understanding of what the different terms in the source function does, and for debugging purposes, we implement the solver in a modular way. We create one method for solving eq. (10) with the source function as an input argument. A second method is implemented for calling the previous method and creating splines of the resulting multipoles calculated using the input source function. This way we can create individual splines for the different multipoles computed using only a specific term from the full source function to see how that specific term contributes to the final result of the C_ℓs. In order to do this we go back to the code from Borg [2020c] and implement a method for computing and splining the full source function from eq. (5). Along side splining the full function, we also makes splines for each of the four terms. In this computation precision is crucial, as most of the debugging for this milestone is through making sure each of these terms are well behaved. In order to do so we create and use splines for as many of the quantities we can directly by the extracting the

[3] From the provided skeleton code.

solutions from the ODE-solver from milestone 3 for the derivative quantities. Only for the quantities we don't have explicit expressions for their derivatives we find the derivatives through the splines of the full quantity.

Computing and splining all the different terms in the source function takes about $\sim 0.5\,\mathrm{s}$, while solving for the multipoles using the full temperature source function is done in $\sim 56\,\mathrm{s}$.

3.3.2 C_ℓ

With the multipoles computed we are ready to handle eq. (2). It is rewritten into and ODE using the logarithm of k and differentiating, resulting in

$$\frac{\mathrm{d}C_\ell(k, x=0)}{\mathrm{d}\log(k)} = 4\pi A_s \left(\frac{k}{k_{\mathrm{pivot}}}\right)^{n_s - 1} \Theta_\ell^2(k, x=0) \tag{11}$$

where we have used $A_s = 2e-9$, $n_s = 0.96$ and $k_{\mathrm{pivot}} = 0.05\,\mathrm{Mpc}^{-1}$. Again we have to specify the initial condition, being for the lowest k value we have in our grid of $k_{\mathrm{min}} = 5 \times 10^{-5}\,\mathrm{Mpc}^{-1}$. Approximating this to $k_{\mathrm{min}} \approx 0$ we see that the evaluated integral essentially goes from $k = 0$ to $k \approx 0$, resulting in zero. Thus we take the initial condition to be zero,

$$C_\ell(k_{\mathrm{min}}, x=0) = 0.$$

This is solved using the splines created for the multipoles from section 3.3.1. We implement a method for computing everything we need, with an argument specifying if we want to solve the system for the full temperature source function in eq. (5) only, or if we wish to also compute the C_ℓs, and hence the multipoles, for each individual term in the source function separately in addition to the full normal solution. Here we introduce a notation to represent the different solutions and terms. The full proper solution using the Θ_ℓ^2 obtained from the full temperature source function is denoted TT, while the results obtained using only the different terms in the source function when computing the multipoles are represented by the name of the term introduced in section 2.1.1. SW, ISW, Doppler and Quad are respectively the Sahcs Wolfe, Integrated Sachs Wolfe, Doppler and quadrupolar terms. In addition, we compute the power spectrum using only the visibility function as the source function, denoted g_tilde.

The results are again splined over the angular scales ℓ, giving us good solutions for all the different values of ℓ between $\ell_{\mathrm{min}} = 2$ to $\ell_{\mathrm{max}} = 2000$. Computing the C_ℓs are done in about $\sim 2\,\mathrm{s}$.

3.4 Solving the Matter Power Spectrum

Solving the matter power spectrum is trivial compared to the full CMB power spectrum. Using eqs. (6) to (8) we already have splines for all the required quantities, so we simply implement methods for evaluating all these equations. We compute the full matter power spectrum, along with the components where i is baryons, CDM and radiation respectively. For radiation this is not particularly relevant, but we compute it anyway as it is only a few simple lines of code to add. The density and velocity of the radiation perturbations are defined through the multipoles as $\delta_\gamma = 4\Theta_0$ and $v_\gamma = -3\Theta_1$. As we don't have much to say about the radiation component, this is left out of our results in section 4, but included in appendix B for completeness.

3.4.1 Equality Scale

The equality scale is found easily numerically by implementing a method looping over the high resolution x-array used in the background computations from milestone 1, testing for when $\Omega_R < 0.5$, breaking the loop and storing the x-value where this happens. Then its simple finding the equality scale by eq. (9) inserting $a_{\mathrm{eq}} = e^{x_{\mathrm{eq}}}$.

4 Results

Now for the entire project we have two different run times, dependent on if we only want the proper solution using the full temperature source function or all the other terms as well. For the temperature source function alone

all the computation are done in $\sim 72\,\mathrm{s}$. Computing the multipoles are by far the most time consuming part of the calculations, and if we want the 5 additional power spectrums it takes about $50\,\mathrm{s}$ more for each term. Then the computations for the entire project is done in about 5 to 6 minutes. We have not implemented any parallel processing in this code, as we had trouble installing and getting open MP to run, but this is of course the first optimization that should be done to further improve the precision and speed of the code.

4.1 Transfer Function and Integrand

Figure 1 displays the resulting multipoles we obtain from eq. (10) through the line of sight integration method, for a few significantly different angular scales in our interval. Here we clearly see the oscillatory and dampening effect from the Bessel functions, as the transfer functions look like damped harmonic oscillators. Let the argument to the function be $z = (k\eta_0 - k\eta(x))$, the transfer function being zero for $z < \ell$, peaking at $z \sim \ell$ and oscillating at $z > \ell$ before being damped. It's not simple to understand the source function from this plot, and that will be discussed further in section 4.2.1.

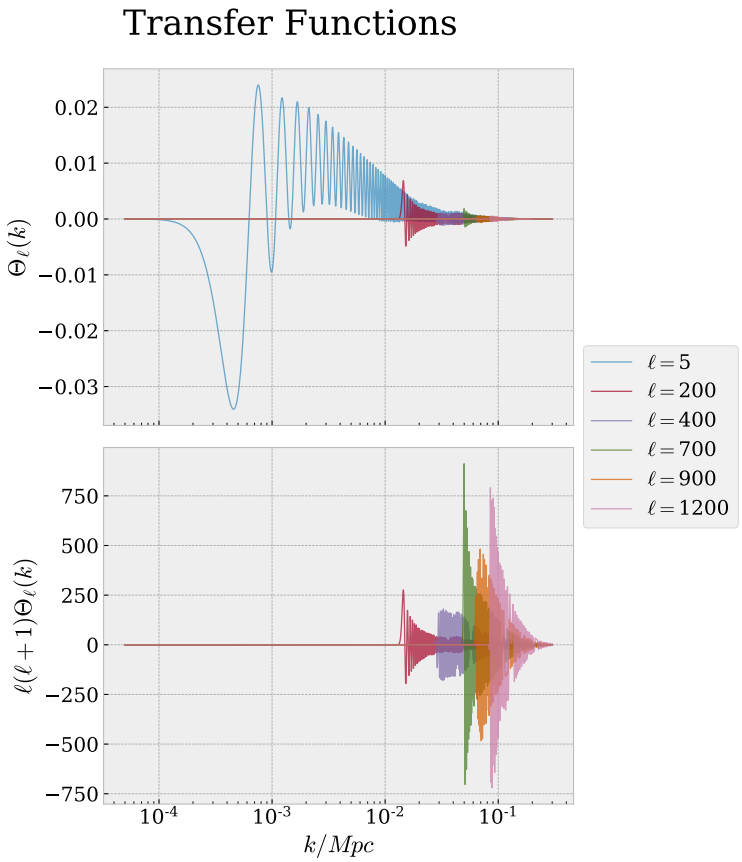

Figure 1: The transfer function Θ_ℓ obtained from line of sight integration in eq. (10) for a few significantly different angular scales. The upper panel shows the unscaled results clearly displaying the large scales. While the lower panel is scaled in a similar way as we will scale the CMB power spectrum, weighted by essentially the square of the angular scale $\ell(\ell + 1)$.

The integrand $\Theta_\ell^2(k)/k$ from eq. (2) are shown in fig. 2. As we essentially see the square of the transfer function, we see much of the same trends, with only positive values, with the larger scales even more dominant as we also divide by the wavenumber. Here we better see how the different scales will affect the power spectrum in the end, and which wavenumbers contributes to the different angular scales. As $k \sim \frac{\ell}{\eta_0}$ this is not so surprising, we see that the larger scales, low ℓ, have a contribution on small k, and vice versa. Here we have not used the same ℓ or normalization, but we see similar results as is presented by Callin in figure 4 [Callin, 2006].

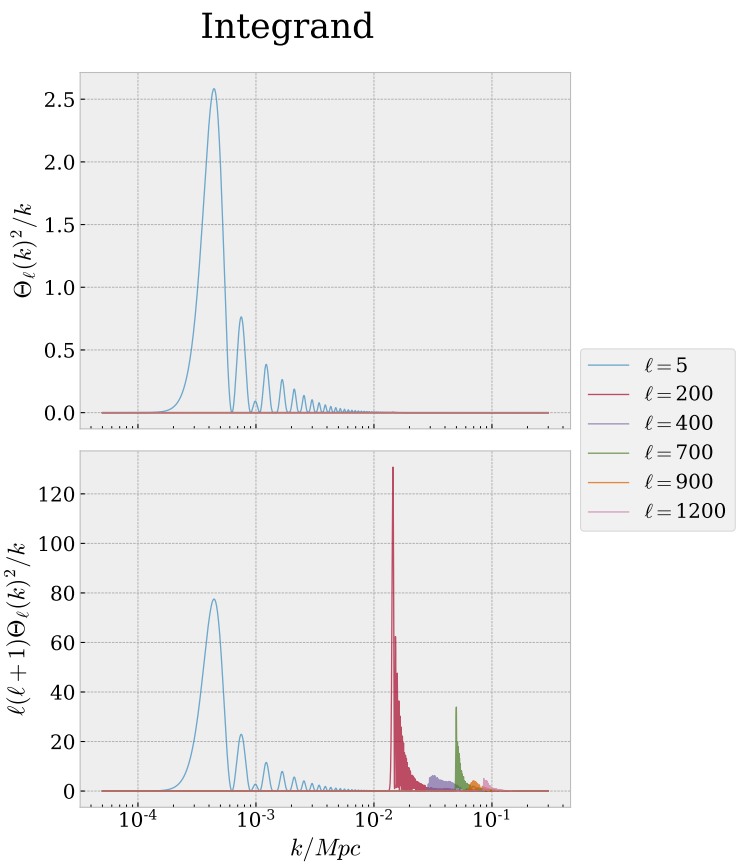

Figure 2: The integrand Θ_ℓ^2/k from eq. (2) for a few significantly different angular scales. The upper panel shows the unscaled results clearly displaying the large scales. While the lower panel is scaled in a similar way as we will scale the CMB power spectrum, weighted by essentially the square of the angular scale $\ell(\ell+1)$.

4.2 Reproducing the CMB Power Spectrum

4.2.1 The Constituent CMB Terms

As discussed in section 2.1.1 we compute the power spectrum obtained from using only the different constituent terms of the full temperature source function in the line of sight integral. This helps us understand the different terms, as well as give us a physical insight in how the different terms and scales contribute. Note that the figure also displays the result from using only the visibility function as the source function, which is a term not actually in the source function by it self, but is only used as a benchmark for our code. This should be a flat spectrum ebbing off at smaller scales, which it indeed does in our result. Using this representation during debugging helped tremendously in backtracking through the code to find which terms where off or implemented wrong.

Here we see that the different terms described in section 2.1.1 behaves as expected. The Sachs Wolfe effect being the main contributor for most scales. The integrated Sachs Wolfe effect contributing much for the largest scales, while the smaller scales contributing many orders of magnitude less, corresponding to the late and early ISW as discussed. The doppler term, which is not weighted by the exponential of the optical depth, contributes more than ISW for all scales except for the largest. This is as expected, as discussed the ISW contributes most on these large scales, while the peculiar velocity of the smaller scales are much higher than for the larger scales at times of recombination, which is where the doppler term is evaluated because of the weighting by the visibility function. We also see how minor the quadrupolar correction term is, being more or less negligible at large scales, but actually larger than the ISW on the smallest scales.

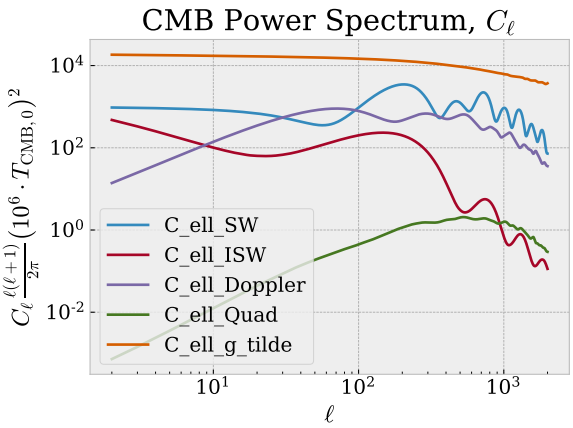

Figure 3: Shown are the resulting C_ℓ using only the individual terms in the source function in the line of sight integration as discussed in section 2.1.1. Note that the full temperature source function is not included here, which is the sum of all the different terms shown except for the g_tilde contribution which is mainly for debugging and benchmarking purposes.

4.2.2 The Final Power Spectrum

The main result, the CMB power spectrum, is shown in fig. 4. Everything we have learned about the different terms, and established throughout these milestones, are now funneled into one single plot. Reading the plot from

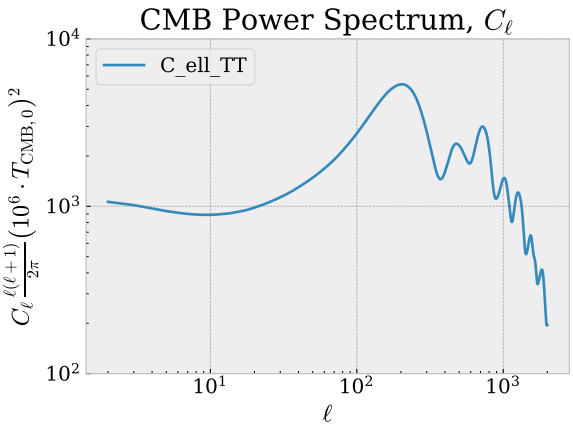

Figure 4: The final reproduced CMB power spectrum, conventionally normalized by $\frac{\ell(\ell+1)}{2\pi} \left(10^6 T_{\mathrm{CMB},0}\right)^2$, so we see $C_\ell \frac{\ell(\ell+1)}{2\pi}$ in units of $\mu\mathrm{K}^2$. This helps better visualize the features of the spectrum, as it generally drops as ℓ^{-2}. Here we see the large scale plateau, the acoustic peak and oscillations and the dampening tail for smaller scales.

large scales to small, we see the plateau on the largest scales, with the late ISW effect contributing to the increase on the very largest scales in $\ell \lesssim 10$. As discussed in Borg [2020c] and in sections 2.1.1 and 4.2.1 this is due to the dark energy dominated regime, where the accelerated expansion halts the growing modes and thus the derivatives of the gravitational potentials are large as we saw in Borg [2020c]. Increasing the dark energy density parameter would cause the dark energy to dominate earlier, and we would have a larger late ISW effect.

Moving on we have the first peak, called the acoustic peak. This is a remnant from the tight coupled regime between baryons and photons in the early perturbations. The baryon-photon fluid traveling as one in the tight coupled regime, before the photons decouple leaving the baryons behind. The baryons are then affected by the gravity of dark matter perturbations, and the baryons affecting the dark matter. The result is a high peak at the $\ell \sim 200$ scale.

On the smaller scales we see how the power spectrum starts to oscillate, called acoustic oscillations, and eventually being exponentially suppressed. Looking at the monopole oscillations from Borg [2020c] we can understand the oscillations, but using the effective monopole which is just a small correction to the monopole

oscillations we looked at in milestone 3. As discussed in Borg [2020c] the equation for the monopole can be characterized as a driven harmonic oscillator. The peaks in the C_ℓ corresponds to scales for which the effective monopole oscillations have a maximum or minimum at the time of recombination, or at the LSS. The troughs in the power spectrum corresponds to scales where the effective monopole is zero at LSS. The photon perturbations characterized by the driven harmonic oscillator equation can be thought of as a simple mass less ball on a spring in a gravitational field, oscillating up and down in a driven motion. If we only had photon perturbations, these oscillations would have been even around the zero point. But as the baryon and photons are heavily coupled, and the baryons having mass in the gravitational field, we can instead think of the oscillator as a ball on a spring, but with mass. The oscillations being due to the balance between gravity and radiation pressure, adding the baryons with mass enhances the compression modes, but not so much the rarification. Thus we get an uneven oscillation, every compression being enhanced, which corresponds to the odd numbered peaks in the power spectrum. This we can clearly see in fig. 4, where the first and third peak being larger than the second and fourth and so on. For higher number peaks this is harder to make out, as the exponential suppression of the power spectrum kicks in. This gives us another insight into determining the cosmological parameters. Measuring the relative height of the even and odd numbered peaks we can infer restrictions on the baryon density parameter.

Last we see the exponential suppression on the smallest scales. This effect is due to photon diffusion, caused by the photons moving in a so called random walk motion through the photon-baryon fluid due to the photons scattering on the free electrons. The average distance the photons travel between each scattering is called the mean free path, $\lambda_{\rm mfp}$, being dependent on the free electron density. Following the central limit theorem, after n scatterings the photons would have moved on average a distance $\lambda_D \sim \sqrt{n}\lambda_{\rm mfp} \sim \frac{1}{\sqrt{n_e \sigma_T H}}$. For perturbations on scales smaller than this distance, the over- and underdensities are able to mix dampening the oscillations. This effect is especially prominent for scales for which the finite thickness of the LSS is not negligible relative perturbation size. This is called diffusion dampening, or silk dampening, exponentially suppressing the anisotropies on scales $\ell \gtrsim 500$. This effect is also dependent on the baryon density parameter because of the scattering, as well as the helium fraction and the number of relativistic particles in our Universe. The latter being determined by the number of massless neutrinos.

4.3 The Matter Power Spectrum

The matter power spectrum is shown in fig. 5. Here we see how the two components overlap each other, as the baryons densities are mostly determined by the gravitational field enforced by the dominant dark matter. For large scales perturbations, we see how the late horizon entry and hence being affected by little causal physics, results in a more or less unprocessed perturbations. We then see a scale dependence consistent with initial perturbations being set up by a gaussian random field, where we expect more perturbations of «medium» scale and less of the super-horizon scales, resulting in the spectrum proportional to k^{n_s}, where the spectral index n_s is close to unity, being determined by the length of the inflationary period.

	Inside	Outside
Radiation era	$\log(a)$	a^2
Matter era	a	a

Table 1: The scale factor dependence for growing matter modes in the radiation and matter dominated eras, inside and outside horizon. These dependencies limits the growth of perturbations on smaller scales, resulting in the peak and the Meszaros suppression observed in fig. 5.

Going to smaller scales we hit the peak in the spectrum, at the equality scale $k_{\rm eq}$ described in eq. (9). This is the scale corresponding to perturbations entering the horizon at the matter-radiation equality. The matter perturbations grows differently with time in the matter and radiation era, and also when being outside and inside the horizon, following the proportionalities listed in table 1. This table shows the evolution of the invariant density in eq. (7). Following the scale factor dependence, or in other words time evolution, we see that modes entering the horizon in the radiation dominated era, before $a_{\rm eq}$, will grow slowly until the matter dominated regime, only $\propto \log(a)$. These scales are therefore suppressed relative to the scales entering after $a_{\rm eq}$, which grows undisturbed as a^2 in the radiation era and a in the matter era. This suppression of the smaller scales is called the Meszaros suppression, and is consistent with our results as we see in fig. 5. For these smaller scales we also se some of the baryonic acoustic oscillations as we saw in the CMB power spectrum. Interestingly these oscillations are also

protruding in the CDM component, again showing that the additional gravitational effect of adding baryons propagates through the coupled system of the Boltzmann-Einstein equations affecting both the photons, as we have seen, and the dark matter perturbations.

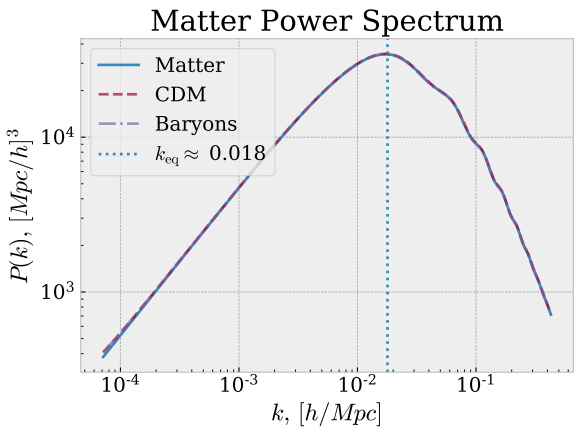

Figure 5: The matter power spectrum, with the components baryons and CDM overplotted and the equality scaled marked in as the vertical dotted line. For larger scales the spectrum goes as $k^{n_s} \sim k^1$, while small scales being suppressed by the Meszaros effect going as k^{n_s-4}, being suppressed by k^{-4} relative to the larger scales entering after matter-radiation equality.

Acknowledgments

The author would like to thank Hans A. Winther for an exciting and interesting course, with an inspiring project and lectures throughout this abnormal semester, and quick and helpful debugging assistance. Thanks to my fellow students for several hours of discussions during the different milestones.

References

GSL Documentation, March 2020. URL `https://www.gnu.org/software/gsl/doc/html/ode-initval.html`.

Jakob Borg. Milestone 1 - The Background Cosmology. Github link to the report included as URL, March 2020a. URL `https://github.com/Lilleborg/AST5220-Cosmology2/blob/master/Numerical_projects/Milestone1/tex/milestone1_jakobbor.pdf`.

Jakob Borg. Milestone 2 - The Recombination History. Github link to the report included as URL, March 2020b. URL `https://github.com/Lilleborg/AST5220-Cosmology2/blob/master/Numerical_projects/Milestone2/tex/jakobbor_Milestone2.pdf`.

Jakob Borg. Milestone 3 - The Evolution of Structure in the Universe. Github link to the report included as URL, March 2020c. URL `https://github.com/Lilleborg/AST5220-Cosmology2/blob/master/Numerical_projects/Milestone3/tex/jakobbor_milestone3.pdf`.

Petter Callin. How to Calculate the CMB Spectrum. June 2006. URL `https://arxiv.org/pdf/astro-ph/0606683.pdf`.

Appendices

A Testing Against Toy Cosmology

As a test of our results we are given a CMB power spectrum and a matter power spectrum using a toy-cosmology in the project description using the parameters $\Omega_{b0} = 0.05$, $\Omega_{\text{CDM0}} = 0.45$, $\Omega_{\Lambda 0} = 0.5$ and $h = 0.7$. Polarization, neutrions, reionization and helium not included, as in our fiducial cosmology.

The CMB results are shown in fig. 6. Here we see that the shape of the spectrum is identical to the one we are presented in the project description. The amplitude of our result seem a bit higher than the test case, but as the shape match to such an extend we are satisfied.

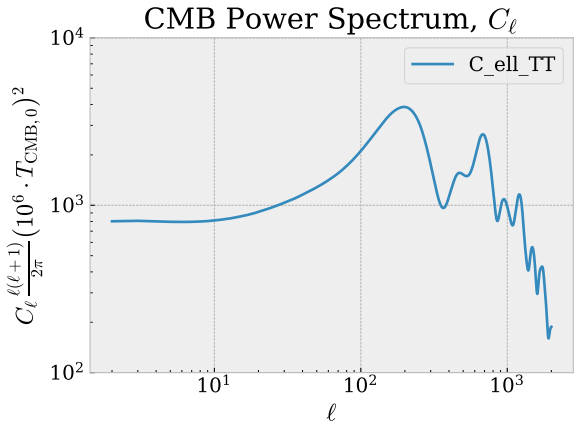

Figure 6: Resulting CMB power spectrum using the toy-cosmology for testing against figure in project description.

The matter results are shown in fig. 7 displaying the matter power spectrum with the matter components overplotted. Again the shape of the spectrum is identical to the test case, with the peak being at approximately the exact same place, while the amplitude is a bit higher. The reason for the higher amplitude in both cases are

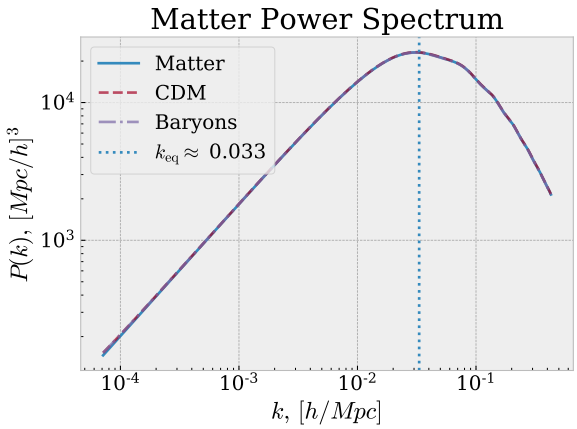

Figure 7: Resulting matter power spectrum using the toy-cosmology for testing against figure in project description. Displayed are the matter power spectrum, with the spectrum from the components baryons and CDM overplotted and the equality scale marked in as the dotted vertical line.

not certain, but it may be due to the way we calculate and introduce the different density parameters. In our code we give the baryon and CDM density parameters as input, but the radiation parameter is calculated using a predefined equation [Borg, 2020a], and finally the parameter for the cosmological constant is calculated from the others. This way we are actually not using the exact same parameters as for the test case, but $\Omega_{\Lambda,0} = 0.49995$ and $\Omega_{R,0} = 5.05 \times 10^{-5}$, which may cause the discrepancy. We have not pursued this further, as forcing $\Omega_{R,0} = 0$

in our code gave very weird results. Another explanation, as we see the inflationary plateau being higher than the test case and we know that this is mostly determined by the initial conditions, is that in some way our initial conditions from milestone 3 or the rescaling done with the primordial power spectrum hides some error or bug.

B The Matter Power Spectrum Components with Radiation

The matter power spectrum with components, including the (for us) irrelevant radiation spectrum. We have little to say about this component, but as we computed it and breifly discussed it in section 2.2 we include the figure here.

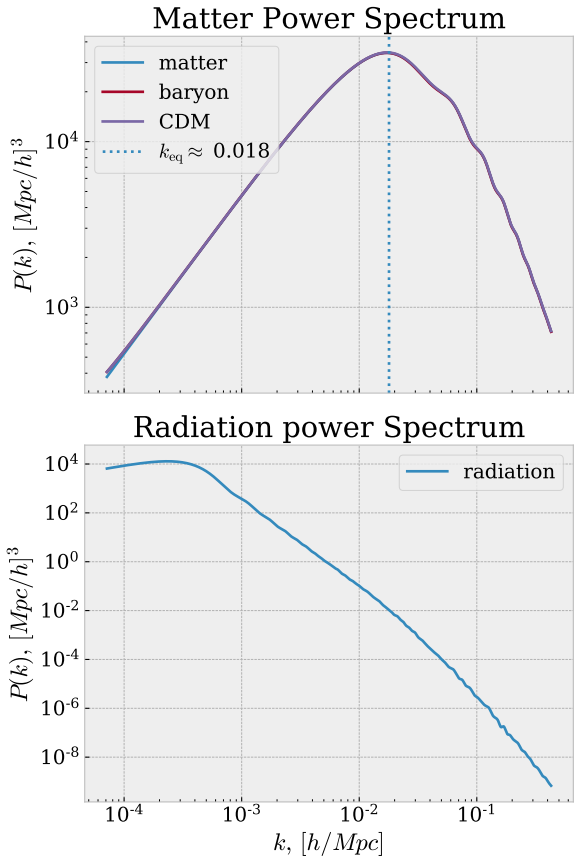

Figure 8: The matter power spectrum components including the radiation power spectrum in the lower panel. The upper panel showing the matter components overplotted the total matter power spectrum, with the equality scale marked as the vertical dotted line.